PHILOSOPHICAL TRANSACTIONS OF THE ROYAL SOCIETY A

rsta.royalsocietypublishing.org

Research

Cite this article: Zhang T, Ma Z, Wang L, Xi J, Shuai Z. 2014 Interface electronic structures of reversible double-docking self-assembled monolayers on an Au(111) surface. *Phil. Trans. R. Soc. A* **372**: 20130018.
http://dx.doi.org/10.1098/rsta.2013.0018

One contribution of 8 to a Theo Murphy Meeting Issue 'Theo Murphy International Scientific Meeting between the UK and China on the chemistry and physics of functional materials'.

Subject Areas:
chemical physics, nanotechnology

Keywords:
self-assembled monolayers, dispersion-corrected density functional theory, work function, interface electronic structure

Author for correspondence:
Zhigang Shuai
e-mail: zgshuai@tsinghua.edu.cn

Electronic supplementary material is available at http://dx.doi.org/10.1098/rsta.2013.0018 or via http://rsta.royalsocietypublishing.org.

Interface electronic structures of reversible double-docking self-assembled monolayers on an Au(111) surface

Tian Zhang[1], Zhongyun Ma[2], Linjun Wang[3], Jinyang Xi[1] and Zhigang Shuai[1]

[1]Key Laboratory of Organic OptoElectronics and Molecular Engineering, Department of Chemistry, Tsinghua University, Beijing 100084, People's Republic of China
[2]School of Aerospace Science and Engineering, National University of Defense Technology, Changsha 410073, People's Republic of China
[3]Service de Chimie des Matériaux Nouveaux, Université de Mons, Place du Parc 20, Mons 7000, Belgium

Double-docking self-assembled monolayers (DDSAMs), namely self-assembled monolayers (SAMs) formed by molecules possessing two docking groups, provide great flexibility to tune the work function of metal electrodes and the tunnelling barrier between metal electrodes and the SAMs, and thus offer promising applications in both organic and molecular electronics. Based on the dispersion-corrected density functional theory (DFT) in comparison with conventional DFT, we carry out a systematic investigation on the dual configurations of a series of DDSAMs on an Au(111) surface. Through analysing the interface electronic structures, we obtain the relationship between single molecular properties and the SAM-induced work-function modification as well as the level alignment between the metal Fermi level and molecular frontier states. The two possible conformations of one type of DDSAM on a metal surface reveal a strong difference in the work-function modification and the electron/hole tunnelling barriers. Fermi-level pinning is found to be a key factor to understand the interface electronic properties.

1. Introduction

Modifying metal electrodes with self-assembled monolayers (SAMs) has a variety of applications in the fields of both organic electronics and molecular electronics [1–6]. Considerable experimental efforts have been made in order to obtain promising SAMs with expected properties to improve device performances [7–10]. In past years, great theoretical progress has been achieved in understanding metal–SAM interface electronic structures [11–14]. By using first-principles calculations, Zojer *et al.* have presented comprehensive studies of various factors impacting on the electronic structures of SAMs, such as the docking group, the backbone, the electron withdrawing/donating ability of polar substituents, the molecular coverage and the mixed ratio of different adsorbed molecules, on work-function modification owing to SAM adsorption and level alignments of the molecular frontier states relative to the metal Fermi level [15–22].

In addition, when the polar substituents of the SAMs can also dock to the metal surface, we arrive at a special type of SAM, namely the double-docking self-assembled monolayers (DDSAMs). Fabrication of well-controlled DDSAMs with either of the two strong docking groups patterning on the metal surface is an experimental challenge. One strategy is adjusting the electrochemical potential of the electrode in the process of chemisorption. Tadjeddine & Flament [23] have shown that it is possible to monitor the flipping of the 4-cyanopyridine (4-CP) adsorbed on an Au(111) single crystal through analysis of the sum frequency generation spectroscopy. The 4-CP stays in its stable stand-up adsorption geometry (on top, via the N atom of the pyridyl group) at the negative potential and is vertically linked (on top, via the N atom of the cyano group) at large positive potential. Another possible approach is to introduce a protecting group into a double-docking molecule (DDMOL) by chemical modification of the stronger docking group. After the chemisorption of SAMs is complete, one needs to return to the original group by removing the protective reagent [24]. Studying these DDSAMs sheds light on a device design strategy of using one kind of molecule to widely tune the charge-carrier injection efficiencies of SAM-modified metal electrodes [14], and the formation of these metal|DDSAM|metal heterojunctions is a prerequisite in the field of molecular electronics for addressing charge transport through molecular junctions [25].

In this work, we study the dual interfacial conformations of a DDSAM using either of its two docking groups bonded to the Au(111) surface. We focus on the impact of the molecular dipole moment reversion arising from the dual configurations on the work-function modification and the level alignment. We note that in conventional density functional theory calculations [26–28] the dispersion interaction was not properly taken into account. As van der Waals (vdW) forces are supposed to be important for the rational design of SAM-based junctions [29], we also perform dispersion-corrected DFT (DFT-D) [30] to investigate the influence of the vdW interaction on the adsorption geometry and further on the electronic structures.

This paper is organized as follows. In §2, we give a brief description of the metal/DDSAM contacts. In §3, we first discuss the adsorption geometries and adsorption energies of the reversible DDSAMs on an Au(111) surface with and without dispersion correction, then we analyse the electronic structures of DDSAMs with no gold present as well as the gold–DDSAM interfaces. Finally, we investigate the work-function modification in relation to the molecular dipole moments and the level alignment with respect to the molecular frontier state energies. Section 4 provides the conclusions of this study.

2. Description of the investigated systems

In figure 1*a*,*b*, we show a schematic of the two conformations of a type of DDSAM absorbed on a metal surface. The three main components of the DDSAM are the first docking group (dock1), the backbone (π) and the second docking group (dock2). The investigated molecules depicted in figure 1*c* are denominated in the following way: *dock1*|*number of rings*|*dock2* (*dock1* is always the docking group bonded to the metal). For the sake of consistency and convenience, we use the same nomenclature when discussing either DDSAMs alone or DDSAMs on a metal surface.

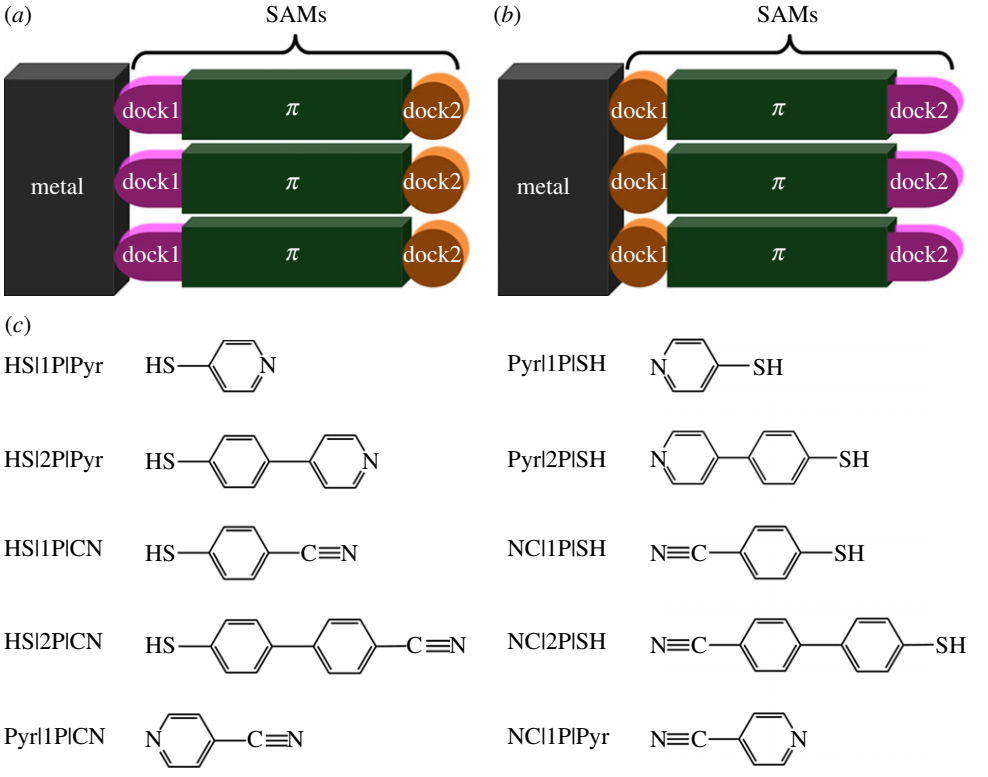

Figure 1. Schematic of (*a*) forward and (*b*) reverse metal/DDSAM contacts. Molecules of the densely packed SAMs consist of three parts: the first docking group (dock1), the π-conjugated backbone (π) and the second docking group (dock2). (*c*) Nomenclatures (dock1|number of rings|dock2) and chemical structures of the molecules studied as DDSAMs on an Au(111) surface. (Online version in colour.)

We choose –SH (thiol), –Pyr (pyridyl) and –CN (cyano) as the docking groups, all of which have been experimentally used as anchoring groups to create single molecular junctions [25,31]. To prevent misunderstanding, a clear distinction should be made here that –NC (isocyano) is also another anchoring group explored extensively but is not covered in this article. The length of the conjugated backbone is varied from one to two rings (1P, 2P). Each type of DDMOL has dual possible configurations to adsorb on the surface (defined as forward and reverse configurations). Note that 4-mercaptopyridine (HS|1P|Pyr), 4-cyanopyridine (Pyr|1P|CN) and cyano-substituted 4-biphenylthiolate (HS|2P|CN) on the Au(111) surface have been subjected to extensive experimental and computational studies for other research objectives [17,21,23,32].

To model a two-dimensional periodic infinite surface in the *xy*-plane, the *repeated-slab* approach is employed [33–35]. Five layers of gold atoms are used to represent the metal surface (figure 2*a*). All DDSAMs are assumed to be packed with a $p\left(\sqrt{3}\times 3\right)$ surface unit cell containing two molecules arranged in a *herringbone* pattern (figure 2*b*) [36]. Details on the DFT-D and DFT calculations using the Vienna *ab initio* Simulation Package (VASP) [37,38] code are reported in the electronic supplementary material.

3. Results and discussion

(a) Adsorption geometry and adsorption energy

After geometry optimizations for all the chosen DDSAMs adsorbed on Au(111), we find that the basic characteristics of the adsorbate structures remain unchanged, i.e. the sulfur docking

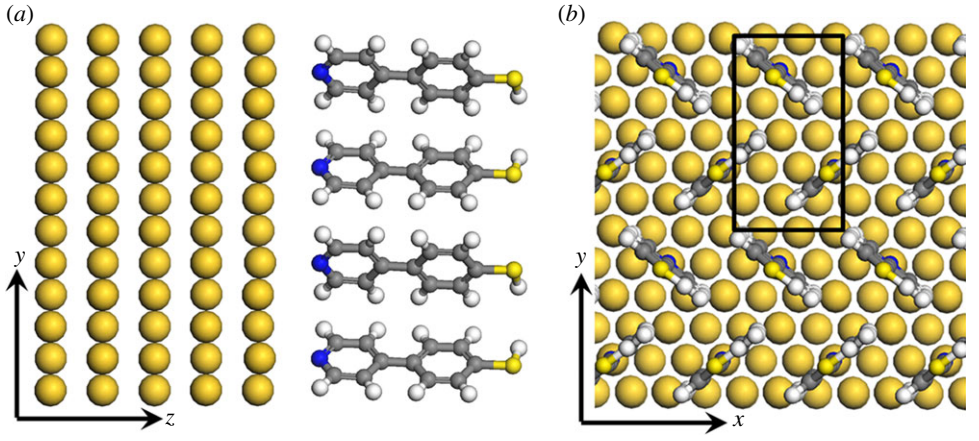

Figure 2. (*a*) Side and (*b*) top views of the representative DDSAMs (Pyr|2P|SH) on the five-layer Au(111) surface. The $p(\sqrt{3} \times 3)$ unit cell with two molecules arranged in a herringbone pattern is marked by the black rectangle in (*b*). (Online version in colour.)

atoms are situated at the *fcc*-hollow sites with a minor distortion towards the bridge sites, while nitrogens stay at the on-top sites as docking atoms. We show the average tilt angles (α) for the molecular long axes relative to the surface normal (see the electronic supplementary material, table S1), which play an important role in the SAM-induced work-function modification [17]. These tilt angles are found to be strongly related to the docking atoms: α is about 13–21° and 0–5° for SAMs with S and N as docking atoms, respectively. In addition, we confirm that the dispersion has almost no impact on the tilt angles, thus previous studies using standard DFT in the absence of vdW corrections are generally safe in predicting the molecular orientations for Au/SAM contacts. However, notable differences do exist between DFT and DFT-D results concerning the average Au–X bond lengths (see the electronic supplementary material, table S1), where X represents the docking atom bonded to gold. Herein, as each S docking atom bonds to three Au atoms, only the shortest Au−S bond length is reported. The DFT calculated $d_{\text{Au-S}}$ is about 2.5 Å, similar to other aromatic thiols on Au(111) [32], while DFT-D gives slightly (about 0.02–0.04 Å) smaller values. When pyridine is used as the docking group binding to gold, the reduction in $d_{\text{Au-N}}$, as high as 0.15–0.29 Å, is much more significant. Note that the DFT-D calculated $d_{\text{Au-N}}$ is about 2.47–2.49 Å, which is in very good agreement with the previous theoretical result (approx. 2.46 Å) obtained by Bilić *et al.* [39] and Hou *et al.* [40] for the pyridine molecules adsorbed onto the Au(111) surface in the on-top configuration. The role of dispersion is exactly opposite with cyano as the docking group binding to gold, where DFT-D gives an approximately 0.1 Å larger $d_{\text{Au-N}}$ than DFT. The calculated $d_{\text{Au-N}}$ for NC|1P|SH and NC|1P|Pyr is 3.22 Å, in line with the typical Au−N (NC) lengths for shorter electrode separations found by Hong *et al.* [25] when studying single molecular junctions, where a tolane derivative bridges between two gold electrodes using cyano anchoring groups.

We report the adsorption energy per molecule, E_{ads}, at both the DFT and DFT-D levels (see the electronic supplementary material, table S1). For systems with thiol as the docking group binding to gold, the adsorption is supposed to happen by replacing the covalent S−H bonds by the S−Au bonds [41]. We define E_{ads} as

$$E_{\text{ads}} = \frac{[(E_{\text{Au(111)+SAM}} + E_{\text{H}_2}) - (2 \cdot E_{\text{mol}} + E_{\text{Au(111)}})]}{2}. \tag{3.1}$$

Here $E_{\text{Au(111)+SAM}}$ is the energy of the Au/SAM combined system containing two molecules per unit cell, and E_{H_2}, E_{mol} and $E_{\text{Au(111)}}$ are the energies of an isolated hydrogen molecule, a single

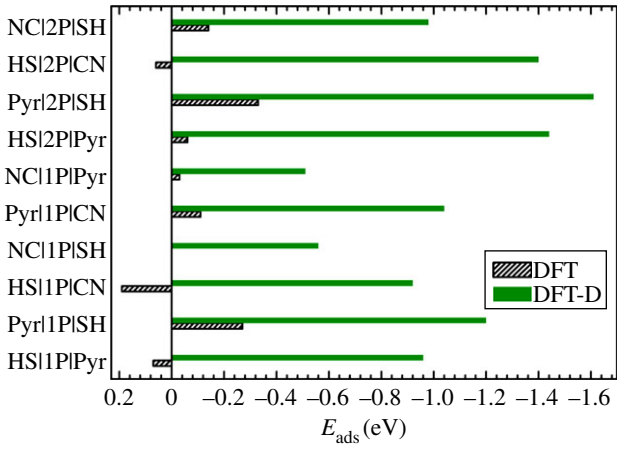

Figure 3. Adsorption energy per molecule adsorbed on an Au(111) surface for all combined systems calculated separately at the DFT and DFT-D levels. (Online version in colour.)

molecule forming the SAM, and the clean Au(111) slab, respectively. For molecules binding to Au(111) via N atoms, E_{ads} can be simply calculated as follows:

$$E_{ads} = \frac{[E_{Au(111)+SAM} - (2 \cdot E_{mol} + E_{Au(111)})]}{2}. \tag{3.2}$$

Concerning E_{ads} calculated by DFT where vdW forces are excluded [35], we find positive values for several investigated systems. This is not surprising because it is well known that a pure DFT generalized gradient approximation (GGA) approach significantly underestimates the adsorption energy of small aromatic molecules on the (111) surfaces of noble metals [42]. Via dispersion correction, all E_{ads} values are markedly reduced (figure 3). The sizable exothermic values indicate that the reversible DDSAMs can indeed be formed on an Au(111) surface and are stable using either of the two docking groups binding to gold. Moreover, the vdW forces also affect the relative energetics of two configurations for the same DDMOLs binding to gold with different docking groups. A representative example is HS|2P|CN and NC|2P|SH, where the standard DFT GGA prefers adsorption via the cyano groups, while dispersion strongly stabilizes the HS|2P|CN configuration. To further discuss the impact of vdW interactions on the adsorption energy per molecule, we analysed the magnitude of DDMOL–metal interactions and the interactions among molecules within the DDSAM separately (see the electronic supplementary material, table S2).

For the same backbone length, we find that the absolute value of E_{ads} generally follows the sequence: Au−Pyr > Au−S > Au−NC [25]. This kind of rule is of essential importance when determining the ratio between the two different conformations using either side of the DDMOLs forming SAMs on gold, and we stress that the correct sequence can be obtained only through considering dispersion effects. Here, it should be mentioned that although vdW forces were accounted for via correction schemes by Grimme [30], a pairwise summation over atom–atom vdW corrections may not be able to give an accurate description of vdW interactions between organic molecules and metal substrates. Note that a more robust method combining the DFT + vdW scheme [43] with the Lifshitz–Zaremba–Kohn (LZK) theory, which includes non-local Coulomb screening within the SAMs, has recently become possible [44].

The geometric and energetic parameters reported in this contribution only provide a reference for the interface structures and conformation stabilities in a static scenario. The entire process of SAM formation is of course more complex and highly dynamic. Both the equilibrium energetics and the kinetics may play important roles. In addition, the precise atomic structure of the interface is still being subjected to scientific debate [14]. We, therefore, limit ourselves to the unreconstructed metal surface and relatively feasible adsorption process.

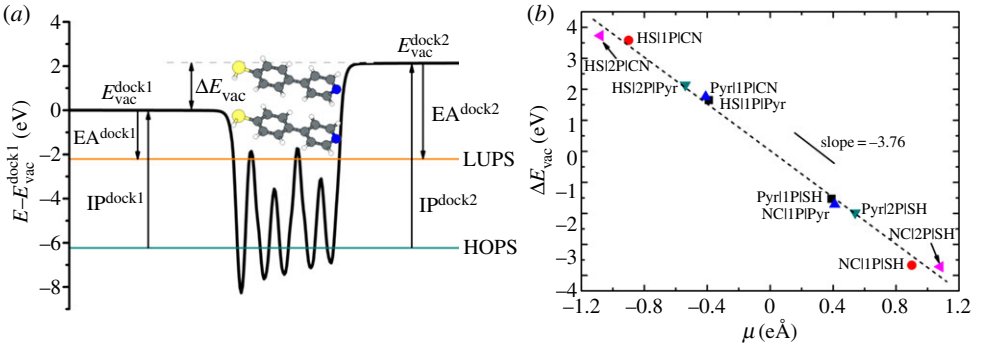

Figure 4. (*a*) Plane(*xy*)-averaged electrostatic potential energy of the free-standing HS|2P|Pyr monolayer. The solid horizontal lines locate the highest occupied π-orbital state (HOPS) and the lowest unoccupied π-orbital state (LUPS). Also indicated are the dock1 and dock2 side vacuum energy levels (E_{vac}^{dock1} and E_{vac}^{dock2}), electrostatic potential energy step across the molecular monolayer ($\Delta E_{vac} = E_{vac}^{dock1} - E_{vac}^{dock2}$), the dock1 and dock2 side ionization potentials (IP^{dock1} and IP^{dock2}), and the corresponding electron affinities (EA^{dock1} and EA^{dock2}). (*b*) ΔE_{vac} as a function of the molecular dipole moment, μ. Data points with the same shape represent DDSAMs with forward and reverse configurations, respectively. A linear fit is performed and shown with a dashed line. (Online version in colour.)

(b) Double-docking self-assembled monolayers in the absence of the gold substrate

We first investigate the electronic structures of the forward and reverse DDSAM conformations with no gold present. HS|2P|Pyr is used as a representative example and all discussions below are based on DFT-D calculations as DFT gives quite similar results. The calculated electron electrostatic potential energies are averaged over the *xy*-plane of the unit cell. In figure 4*a*, the DDSAM divides the space into two regions (dock1 side and dock2 side) with two different vacuum levels (E_{vac}^{dock1} and E_{vac}^{dock2}). The difference between these two levels, ΔE_{vac}, is the electrostatic potential energy step across the dipolar DDSAM, which can also be determined by the heuristic Helmholtz equation [14]

$$\Delta E_{vac} = -\frac{e\mu_{\perp}}{A\varepsilon_0} = -2\frac{e\mu\cos\theta}{A\varepsilon_0\varepsilon_{eff}}. \tag{3.3}$$

Here, e is the elementary charge, $\mu_{\perp}$ denotes the projection of the SAM dipole moment per unit cell onto the surface normal, A is the per unit cell area, μ is the dipole moment of a single isolated molecule in the geometry as it is in the SAM, θ is the average tilt angle of the molecules, ε_0 is the vacuum permittivity and ε_{eff} is the effective depolarization factor to describe the reduction in the dipole moment of each molecule in the SAM rising from the electric field created by the dipole moments of all neighbouring molecules [15,34]. Thus, we can find that the sign of ΔE_{vac} depends on the nature of the permanent dipole moment of the molecules forming the DDSAM. In figure 4*b*, there is a linear relationship between ΔE_{vac} and μ with a slope of $-3.76\,\mathrm{V\,Å^{-1}}$. This demonstrates an almost equivalent $\cos\theta/\varepsilon_{eff}$ for the investigated DDSAMs. Thereby, ΔE_{vac} of the forward and reverse DDSAM conformations are generally of opposite signs and nearly the same absolute values although the molecular tilting angles may be quite different in some cases (see the electronic supplementary material, table S1).

To construct a smooth transport channel through the SAM, we need to pick out the most suitable frontier states, i.e. the highest occupied π-state (HOPS) and the lowest unoccupied π-state (LUPS) [21]. This means that the nature of the states associated with the peaks in the density of states needs to be carefully identified. For all the investigated DDSAMs, the lowest unoccupied states are always of π character, and thus it is unambiguous to define the LUPS. However, for DDSAMs with pyridine docking groups, the highest occupied orbital is of σ character [39], and therefore one needs to dig further to lower energy levels to find the π-state delocalized over the molecular backbone (see the electronic supplementary material, figures S3–S5). Considering

Table 1. Electronic structure of the free-standing DDSAMs: μ is the dipole moment of molecules in the geometry as they adopt in the SAM; ΔE_{vac} is the electrostatic potential energy step across the molecular monolayer; IP^{dock1} and EA^{dock1} are the dock1 side ionization potential and electron affinity; IP^{dock2} and EA^{dock2} are the dock2 side ionization potential and electron affinity. All energetic parameters are calculated at the DFT-D level.

systems	μ (eÅ)	ΔE_{vac} (eV)	IP^{dock1} (eV)	EA^{dock1} (eV)	IP^{dock2} (eV)	EA^{dock2} (eV)
HS|1P|Pyr	−0.39	1.65	6.25	1.66	7.89	3.30
Pyr|1P|SH	0.39	−1.53	7.96	3.29	6.43	1.76
HS|1P|CN	−0.90	3.58	5.35	1.81	8.94	5.39
NC|1P|SH	0.90	−3.67	9.14	5.58	5.47	1.91
Pyr|1P|CN	−0.41	1.76	8.08	3.87	9.84	5.62
NC|1P|Pyr	0.41	−1.71	9.81	5.61	8.10	3.90
HS|2P|Pyr	−0.54	2.14	6.23	2.21	8.37	4.35
Pyr|2P|SH	0.54	−1.98	8.41	4.31	6.43	2.33
HS|2P|CN	−1.08	3.73	5.14	2.32	8.87	6.05
NC|2P|SH	1.08	−3.72	8.99	6.16	5.27	2.45

the fact that an electron can be removed from HOPS to vacuum at either the dock1 side or the dock2 side, we obtain two different ionization potentials, IP^{dock1} and IP^{dock2}. Similarly, we also have two electron affinities, EA^{dock1} and EA^{dock2}, representing the addition of an electron from vacuum to the LUPS. It is straightforward to see that IP^{dock1} (EA^{dock1}) for the forward DDSAMs is almost the same as IP^{dock2} (EA^{dock2}) for the corresponding reverse DDSAMs (table 1). Note that we find almost the same evolution of ΔE_{vac} with respect to μ as well as IP and EA values using DFT rather than DFT-D (see the electronic supplementary material, table S3 and figure S1), implying that vdW has a negligible effect on the free-standing DDSAM properties.

(c) Bond dipole at the gold–double-docking self-assembled monolayer interface

As is discussed previously, for the DDSAMs adsorbed on gold via the sulfur atoms of the thiols, the S−H bonds are replaced by the S−Au bonds. As a result, the *xy*-plane integrated charge-density rearrangement, $\Delta\rho(z)$, occurring at the gold–SAM interface upon bond formation, is given by [15,35,41]

$$\Delta\rho(z) = \rho_{Au(111)+SAM}(z) - \{[\rho_{SAM}(z) - \rho_H(z)] + \rho_{Au(111)}(z)\}, \tag{3.4}$$

where $\rho_{Au(111)+SAM}(z)$, $\rho_{SAM}(z)$, $\rho_{Au(111)}(z)$ and $\rho_H(z)$ are the *xy*-plane integrated charge density of the combined gold/SAM system, the free-standing monolayer saturated with hydrogens, the gold slab alone and the hydrogen-atom layer, respectively. For the DDSAMs binding to gold via the nitrogen atoms of the pyridyls or the cyanos, the expression reads [14]

$$\Delta\rho(z) = \rho_{Au(111)+SAM}(z) - [\rho_{SAM}(z) + \rho_{Au(111)}(z)]. \tag{3.5}$$

Here, $\rho_{SAM}(z)$ is simply the charge density of the SAM without substituting additional hydrogens.The net charge transfer, $\Delta Q(z)$, specifying the total amount of electrons moved from the right-hand side of a plane at position z to the left-hand side of that plane, can be calculated as

$$\Delta Q(z) = \int_{-\infty}^{z} \Delta\rho(z')dz'. \tag{3.6}$$

And the electron potential energy step, $\Delta E(z)$, can be evaluated by solving the one-dimensional Poisson equation based on $\Delta\rho(z)$

$$\frac{d^2\Delta E(z)}{dz^2} = \frac{e}{\varepsilon_0 A}\Delta\rho(z). \tag{3.7}$$

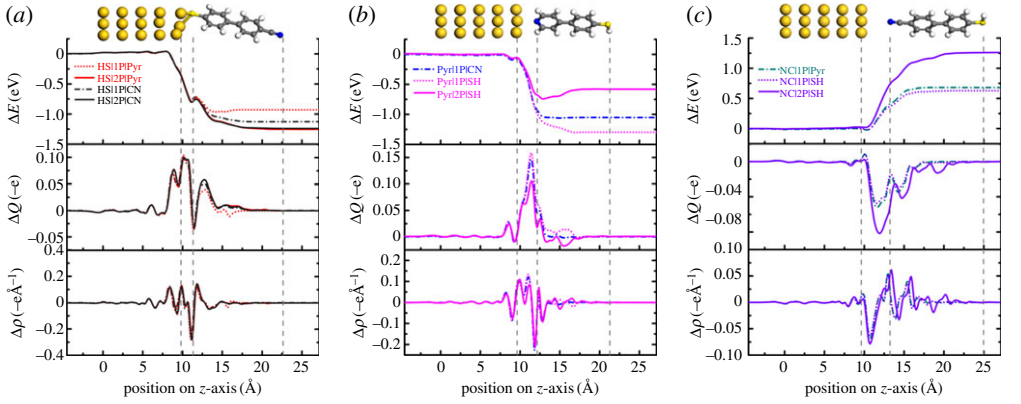

Figure 5. (x, y)-plane integrated charge-density rearrangements between the gold substrate and the DDSAMs, $\Delta\rho$, net charge transfer, ΔQ, as well as the resulting electrostatic potential energy, ΔE, for the systems with one (dotted and dashed lines) and two (solid line) rings. Situations for different dock1 groups (−SH, −Pyr and −CN) are separately included in (*a*), (*b*) and (*c*), respectively. The vertical dashed lines indicate the positions of the top gold layer, the atom docking to the substrate and the top-most atom of the molecules, respectively. (Online version in colour.)

The bond dipole, ΔE_{BD}, defined as the electron potential energy difference between the gold surface vacuum and the dock1 side vacuum, is strongly related to the charge redistribution at gold–SAM interfaces. We plot $\Delta\rho(z)$, $\Delta Q(z)$ and $\Delta E(z)$ calculated at the DFT-D level for typical DDSAMs adsorbed on gold with three different docking groups binding to gold (figure 5). Using thiols and pyridyls bonded to gold, $\Delta\rho_{\mathrm{BD}}$ is very much localized in the immediate region between the docking groups and the adjacent gold layers, and $\Delta Q(z)$ drops to zero in the vicinity of the dock1 groups, implying negligible net charge transfer between gold and these SAMs. By contrast, SAMs with cyanos as docking groups, significant long-range charge transfer between gold and the SAM is observed, and a net charge transfer as high as −0.06 e is achieved mainly because of the strong electron withdrawing ability of the cyano groups [45]. As a type of DDSAM can absorb onto gold with two different docking groups, distinct values of ΔE_{BD} are observed for the two different configurations (table 2). Besides, we find pronounced differences in ΔE_{BD} values calculated by DFT in comparison with DFT-D (see the electronic supplementary material, table S4). As discussed previously, dispersion has a strong impact on the bond lengths at the interface, thus these differences imply that ΔE_{BD} is quite sensitive to the interface geometries [46].

(d) Work-function modification

As is well known, the work-function modification owing to SAM adsorption, $\Delta\Phi$, is the summation of ΔE_{vac} and ΔE_{BD} [8]

$$\Delta\Phi = \Delta E_{\mathrm{vac}} + \Delta E_{\mathrm{BD}}. \tag{3.8}$$

We give all the calculated $\Delta\Phi$ at the DFT-D level (table 2) and plot $\Delta\Phi$ as a function of the molecular dipole moment μ in figure 6. We observe a strong correlation between $\Delta\Phi$ and μ as ΔE_{vac} is almost linear with μ, and the ΔE_{BD} for the investigated systems are generally smaller in magnitude than the ΔE_{vac}. As is expected, SAMs with relatively large dipole moments, i.e. the systems of NC|1P|SH, HS|1P|CN, NC|2P|SH and HS|2P|CN (table 1), tend to achieve large work-function modifications. However, when a system (e.g. Pyr|1P|SH and Pyr|2P|SH) poses the same sign for ΔE_{BD} and ΔE_{vac}, even a relatively small μ could achieve a large $\Delta\Phi$. Similarly, when systems pose opposite signs but similar absolute magnitude for ΔE_{BD} and ΔE_{vac}, such as HS|2P|Pyr, Pyr|1P|CN and HS|1P|Pyr, very small $\Delta\Phi$ are obtained. We achieve significantly different work-function modifications for the two different conformations based on

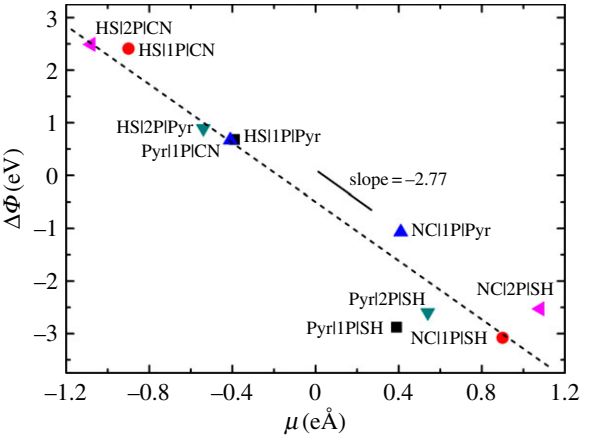

Figure 6. Dependence of the work-function modification, $\Delta\Phi$, on the molecular dipole moment, μ. Data points with the same shape represent forward and reverse combined systems, respectively. (Online version in colour.)

Table 2. Electronic properties of the DDSAMs on Au(111): ΔE_{BD} is the bond-dipole-induced interfacial potential energy shift; $\Delta\Phi$ is the SAM-induced work-function modification; $\Delta E_{HOPS}/\Delta E_{LUPS}$ is the alignment of the frontier molecular π/π^* states delocalized over the backbone with the metal Fermi level; IP^{SAM}/EA^{SAM} is the ionization potential/electron affinity of the bonded SAM defined as the energetic difference between the HOPS/LUPS peak and the vacuum level. All energetic parameters are obtained at the DFT-D level.

systems	ΔE_{BD} (eV)	$\Delta\Phi$ (eV)	ΔE_{HOPS} (eV)	ΔE_{LUPS} (eV)	IP^{SAM} (eV)	EA^{SAM} (eV)
HS|1P|Pyr	−0.93	0.68	−1.94	2.72	7.82	3.16
Pyr|1P|SH	−1.31	−2.88	−3.38	0.70	5.74	1.66
HS|1P|CN	−1.13	2.41	−1.01	2.62	8.62	4.99
NC|1P|SH	0.63	−3.08	−3.27	0.28	5.42	1.87
Pyr|1P|CN	−1.05	0.67	−3.95	0.33	9.86	5.58
NC|1P|Pyr	0.69	−1.07	−4.04	0.30	8.21	3.87
HS|2P|Pyr	−1.26	0.89	−1.80	1.91	7.89	4.18
Pyr|2P|SH	−0.59	−2.60	−2.72	0.26	5.36	2.37
HS|2P|CN	−1.24	2.49	−0.95	1.77	8.65	5.92
NC|2P|SH	1.26	−2.53	−2.55	0.28	5.26	2.43

the same DDMOL because the molecular dipole moments in these two cases are of opposite directions. A similar relationship could also be obtained through DFT calculations, although some calculated $\Delta\Phi$ are slightly different from those calculated at the DFT-D level (see the electronic supplementary material, table S4 and figure S2). Note that the calculated $\Delta\Phi$ here should be considered as an upper limit for the experimentally observed values because it is generally difficult to achieve the high-coverage SAMs for dipolar molecules, as assumed in the present calculations [47].

(e) Level alignment and Fermi-level pinning

The level alignments of delocalized frontier molecular states relative to the gold Fermi level, ΔE_{HOPS} and ΔE_{LUPS}, are essential for understanding the charge injection efficiency of SAM-modified gold electrodes. Here, the well-known deficiencies of (semi)local DFT (as well as

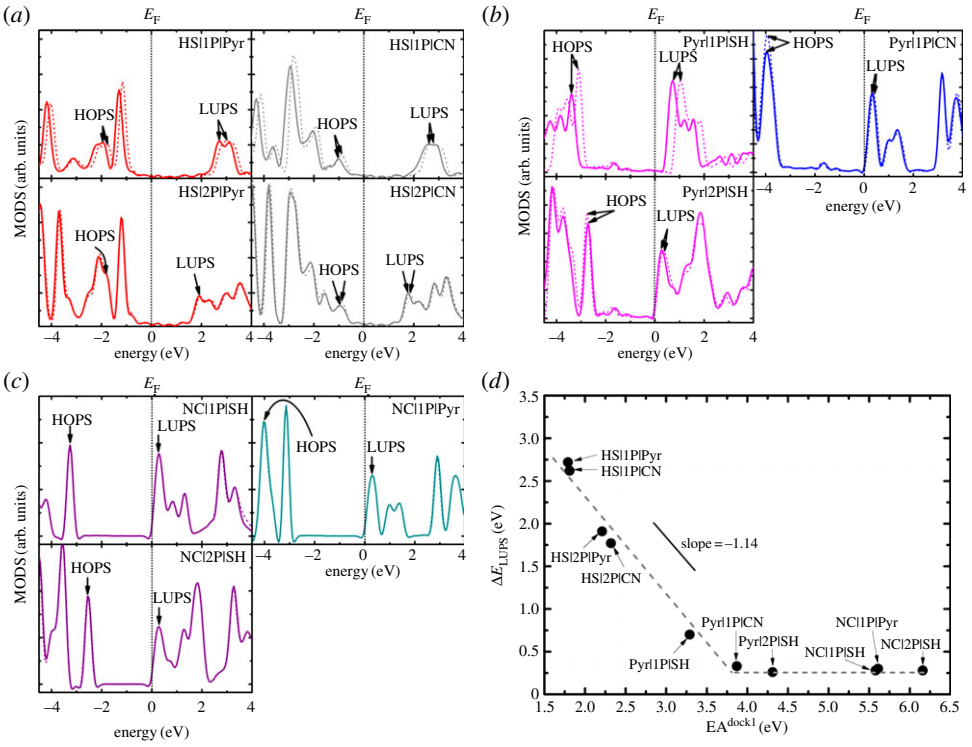

Figure 7. Density of states projected onto the molecular region (MDOS) of the combined gold/SAM systems with (*a*) thiols, (*b*) pyridyls and (*c*) cyanos docking to the Au(111) surface based on DFT-D (solid line) and DFT (dashed line) calculations. The arrows indicate the positions of the HOPS and the LUPS. The Fermi levels are aligned to zero. (*d*) Energy difference between the LUPS in the bonded SAM and the Fermi level of metal, ΔE_{LUPS}, as a function of the dock1 side electron affinities, EA^{dock1}. The energetic parameters are from DFT-D calculations. (Online version in colour.)

DFT-D) in predicting energy levels need to be addressed. The lack of derivative discontinuity of the exchange–correlation functional combined with self-interaction error results in an underestimated energy band gap [48]. However, surface screening, which is partly missing in the conventional DFT (as well as the DFT-D), could reduce this gap [49]. Thus, the error of the present results is at least partially offset and the relative magnitude of the energy levels should not be strongly affected. Similar to determining the HOPS and LUPS of the free-standing monolayers, we perform a careful examination of the peaks of the density of states projected onto the molecular region (MDOS) by DFT and DFT-D (see the electronic supplementary material, figures S6–S8) and pick out the delocalized frontier molecular states in the bonded SAM, i.e. HOPS and LUPS (figure 7*a–c*). We can see that the MDOS for some DDSAMs with backbone 1P calculated from DFT does not coincide with DFT-D results (figure 7*a*,*b*). As listed in table 2, we find that the charge-carrier injection for DDSAM-modified gold can be hole-injection favoured ($|\Delta E_{HOPS}| < |\Delta E_{LUPS}|$) or electron-injection favoured ($|\Delta E_{HOPS}| > |\Delta E_{LUPS}|$). In a lot of cases, e.g. HS|2P|CN versus NC|2P|SH, one configuration could be hole-injection favoured, while the other configuration of the same kind of DDMOL on the gold surface is more electron-injection favoured. Thus using DDSAMs, we can even tune the charge-carrier type through the gold/SAM junction using only one kind of DDMOL.

In table 2, five investigated systems, i.e. NC|1P|SH, Pyr|1P|CN, NC|1P|Pyr, Pyr|2P|SH and NC|2P|SH, pose very similar ΔE_{LUPS} (approx. 0.30 eV). Such small values of ΔE_{LUPS} are very helpful for electron transport with the SAM-modified gold electrode. A more systematic picture evolves when plotting ΔE_{LUPS} as a function of dock1 side electron affinities EA^{dock1} (figure 7*d*).

There is a clear linear evolution (slope = −1.14) of ΔE_{LUPS} with respect to $\mathrm{EA}^{\mathrm{dock1}}$ when $\mathrm{EA}^{\mathrm{dock1}}$ is smaller than approximately 3.75 eV. Further increasing in $\mathrm{EA}^{\mathrm{dock1}}$, ΔE_{LUPS} reaches a plateau, implying that the Fermi level of gold is pinned by the LUPS of the SAM. Such Fermi-level pinning has been observed for a lot of SAMs on gold [15,21]. When the LUPS of the SAM falls below the gold Fermi level, a portion of the electron will transfer to the SAM. As the LUPS is delocalized over the entire SAM, even a small net amount of charge transfer gives rise to a significant bond dipole, which shifts down the gold Fermi level relative to the LUPS of the SAM. Consequently, electron equilibrium is established, and the final Fermi level gets pinned at the onset of the LUPS of the SAM. Here, it should be mentioned that as DFT (as well as DFT-D) gives too low-lying unoccupied states, Fermi-level pinning may not be guaranteed to occur in the very systems of this contribution; however, the obtained fundamental trends should be generally correct. Concerning our study using DDSAMs, we find that the Fermi level of gold is able to be pinned at two different energies as the DDSAMs form two configurations on gold with different values of $\mathrm{EA}^{\mathrm{dock1}}$. Tuning the ratio of these two conformations enables us to tune the Fermi level of a modified gold electrode for a wide range with the same kind of DDMOLs.

4. Conclusion

To summarize, we have presented a comprehensive study on a series of reversible DDSAMs on an Au(111) surface at both the DFT-D and the DFT levels. We have found that vdW interactions have a negligible impact on the molecular tilt angles but can strongly influence the bonding between gold and the SAMs. We have elucidated the difference in electronic properties of the forward and reverse conformations. Especially, we have found that by choosing different docking groups bonded to gold, it is possible to achieve either a decrease or an increase in the gold work function, to build an electron- or a hole-favourable gold/SAM contact, and to pin the gold Fermi level at different energies. Thus, we have confirmed that DDSAMs are promising materials to modify gold electrodes for multi-functional applications. Finally, we note that, owing to the similar adsorption energy for the dual conformations of DDSAMs, it is possible to form a monolayer of mixed conformations, the study of which is currently underway.

Acknowledgements. T.Z. is deeply indebted to Dr Ferdinand Rissner and Dr Georg Heimel for extensive discussions. The authors thank Dr Peng Cui for the help concerning DFT-D calculations and Prof. J. N. H. Reek and Prof. J. Huskens for fruitful discussions about the experiments.

Funding statement. Financial support from the Innovative Research Groups of the National Natural Science Foundation of China (grant nos. 21121004) and the Ministry of Science and Technology of China through the 973 program (grant nos. 2011CB932304, 2011CB808405 and 2013CB933500) are gratefully acknowledged.

References

1. Chen J, Reed MA, Rawlett AM, Tour JM. 1999 Large on-off ratios and negative differential resistance in a molecular electronic device. *Science* **286**, 1550–1552. (doi:10.1126/science.286.5444.1550)
2. Love JC, Estroff LA, Kriebel JK, Nuzzo RG, Whitesides GM. 2005 Self-assembled monolayers of thiolates on metals as a form of nanotechnology. *Chem. Rev.* **105**, 1103–1169. (doi:10.1021/cr0300789)
3. Akkerman HB, Blom PWM, de Leeuw DM, de Boer B. 2006 Towards molecular electronics with large-area molecular junctions. *Nature* **441**, 69–72. (doi:10.1038/nature04699)
4. Dichtel WR, Heath JR, Fraser Stoddart J. 2007 Designing bistable [2]rotaxanes for molecular electronic devices. *Phil. Trans. R. Soc. A* **365**, 1607–1625. (doi:10.1098/rsta.2007.2034)
5. Weiss EA, Kriebel JK, Rampi M-A, Whitesides GM. 2007 The study of charge transport through organic thin films: mechanism, tools and applications. *Phil. Trans. R. Soc. A* **365**, 1509–1537. (doi:10.1098/rsta.2007.2029)
6. Kronemeijer AJ, Akkerman HB, Kudernac T, van Wees BJ, Feringa BL, Blom PWM, de Boer B. 2008 Reversible conductance switching in molecular devices. *Adv. Mater.* **20**, 1467–1473. (doi:10.1002/adma.200800053)

7. De Renzi V, Rousseau R, Marchetto D, Biagi R, Scandolo S, del Pennino U. 2005 Metal work-function changes induced by organic adsorbates: a combined experimental and theoretical study. *Phys. Rev. Lett*. **95**, 046804. (doi:10.1103/PhysRevLett.95.046804)
8. de Boer B, Hadipour A, Mandoc MM, van Woudenbergh T, Blom PWM. 2005 Tuning of metal work functions with self-assembled monolayers. *Adv. Mater.* **17**, 621–625. (doi:10.1002/adma.200401216)
9. Asadi K, Gholamrezaie F, Smits ECP, Blom PWM, de Boer B. 2007 Manipulation of charge carrier injection into organic field-effect transistors by self-assembled monolayers of alkanethiols. *J. Mater. Chem.* **17**, 1947–1953. (doi:10.1039/b617995a)
10. Kind M, Wöll C. 2009 Organic surfaces exposed by self-assembled organothiol monolayers: preparation, characterization, and application. *Prog. Surf. Sci.* **84**, 230–278. (doi:10.1016/j.progsurf.2009.06.001)
11. Ishii H, Sugiyama K, Ito E, Seki K. 1999 Energy level alignment and interfacial electronic structures at organic/metal and organic/organic interfaces. *Adv. Mater.* **11**, 605–625. (doi:10.1002/(sici)1521-4095(199906)11:8<605::aid-adma605>3.0.co;2-q)
12. Bilié A, Reimers JR, Hush NS. 2005 The structure, energetics, and nature of the chemical bonding of phenylthiol adsorbed on the Au(111) surface: implications for density-functional calculations of molecular-electronic conduction. *J. Chem. Phys.* **122**, 094708. (doi:10.1063/1.1850455)
13. Rusu PC, Giovannetti G, Brocks G. 2007 Dipole formation at interfaces of alkanethiolate self-assembled monolayers and Ag(111). *J. Phys. Chem. C* **111**, 14 448–14 456. (doi:10.1021/jp073420k)
14. Heimel G, Rissner F, Zojer E. 2010 Modeling the electronic properties of π-conjugated self-assembled monolayers. *Adv. Mater.* **22**, 2494–2513. (doi:10.1002/adma.200903855)
15. Heimel G, Romaner L, Zojer E, Brédas J-L. 2007 Toward control of the metal-organic interfacial electronic structure in molecular electronics: a first-principles study on self-assembled monolayers of π-conjugated molecules on noble metals. *Nano Lett.* **7**, 932–940. (doi:10.1021/nl0629106)
16. Romaner L, Heimel G, Zojer E. 2008 Electronic structure of thiol-bonded self-assembled monolayers: impact of coverage. *Phys. Rev. B* **77**, 045113. (doi:10.1103/PhysRevLett.102.073005)
17. Wang L, Rangger GM, Romaner L, Heimel G, Buèko T, Ma Z, Li Q, Shuai Z, Zojer E. 2009 Electronic structure of self-assembled monolayers on Au(111) surfaces: the impact of backbone polarizability. *Adv. Funct. Mater.* **19**, 3766–3775. (doi:10.1002/adfm.200901152)
18. Egger DA, Rissner F, Rangger GM, Hofmann OT, Wittwer L, Heimel G, Zojer E. 2010 Self-assembled monolayers of polar molecules on Au(111) surfaces: distributing the dipoles. *Phys. Chem. Chem. Phys.* **12**, 4291–4294. (doi:10.1039/b924238b)
19. Rissner F, Egger DA, Romaner L, Heimel G, Zojer E. 2010 The electronic structure of mixed self-assembled monolayers. *ACS Nano* **4**, 6735–6746. (doi:10.1021/nn102360d)
20. Wang L, Rangger GM, Ma Z, Li Q, Shuai Z, Zojer E, Heimel G. 2010 Is there a Au-S bond dipole in self-assembled monolayers on gold? *Phys. Chem. Chem. Phys.* **12**, 4287–4290. (doi:10.1039/b924306m)
21. Ma Z, Rissner F, Wang L, Heimel G, Li Q, Shuai Z, Zojer E. 2011 Electronic structure of pyridine-based SAMs on flat Au(111) surfaces: extended charge rearrangements and Fermi level pinning. *Phys. Chem. Chem. Phys.* **13**, 9747–9760. (doi:10.1039/c0cp02168g)
22. Rissner F, Ma Z, Hofmann OT, Slugovc C, Shuai Z, Zojer E. 2012 Radical self-assembled monolayers on Au(111) formed by the adsorption of closed-shell molecules. *J. Mater. Chem.* **22**, 4269–4272. (doi:10.1039/c2jm15056e)
23. Tadjeddine M, Flament JP. 2001 *Ab initio* interpretation of sum frequency generation spectra of 4-cyanopyridine adsorbed on Au(111). *Chem. Phys.* **265**, 27–46. (doi:10.1016/S0301-0104(01)00240-3)
24. Díez-Pérez I, Hihath J, Lee Y, Yu L, Adamska L, Kozhushner MA, Oleynik II, Tao N. 2009 Rectification and stability of a single molecular diode with controlled orientation. *Nat. Chem.* **1**, 635–641. (doi:10.1038/nchem.392)
25. Hong W, Manrique DZ, Moreno-García P, Gulcur M, Mishchenko A, Lambert CJ, Bryce MR, Wandlowski T. 2012 Single molecular conductance of tolanes: experimental and theoretical study on the junction evolution dependent on the anchoring group. *J. Am. Chem. Soc.* **134**, 2292–2304. (doi:10.1021/ja209844r)

26. Perdew JP, Chevary JA, Vosko SH, Jackson KA, Pederson MR, Singh DJ, Fiolhais C. 1992 Atoms, molecules, solids, and surfaces: applications of the generalized gradient approximation for exchange and correlation. *Phys. Rev. B* **46**, 6671–6687. (doi:10.1103/PhysRevB.46.6671)
27. Perdew JP, Wang Y. 1992 Accurate and simple analytic representation of the electron-gas correlation energy. *Phys. Rev. B* **45**, 13 244–13 249. (doi:10.1103/PhysRevB.45.13244)
28. Perdew JP, Burke K, Ernzerhof M. 1996 Generalized gradient approximation made simple. *Phys. Rev. Lett.* **77**, 3865–3868. (doi:10.1103/PhysRevLett.77.3865)
29. Nerngchamnong N, Yuan L, Qi D-C, Li J, Thompson D, Nijhuis CA. 2013 The role of van der Waals forces in the performance of molecular diodes. *Nat. Nanotechnol.* **8**, 113–118. (doi:10.1038/nnano.2012.238)
30. Grimme S. 2006 Semiempirical GGA-type density functional constructed with a long-range dispersion correction. *J. Comput. Chem.* **27**, 1787–1799. (doi:10.1002/jcc.20495)
31. Kiguchi M, Kaneko S. 2013 Single molecule bridging between metal electrodes. *Phys. Chem. Chem. Phys.* **15**, 2253–2267. (doi:10.1039/c2cp43960c)
32. Ramírez EA, Cortés E, Rubert AA, Carro P, Benítez G, Vela ME, Salvarezza RC. 2012 Complex surface chemistry of 4-mercaptopyridine self-assembled monolayers on Au(111). *Langmuir* **28**, 6839–6847. (doi:10.1021/la204951u)
33. Sun Q, Selloni A, Scoles G. 2006 Electronic structure of metal/molecule//metal junctions: a density functional theory study of the influence of the molecular terminal group. *J. Phys. Chem. B* **110**, 3493–3498. (doi:10.1021/jp053673i)
34. Natan A, Zidon Y, Shapira Y, Kronik L. 2006 Cooperative effects and dipole formation at semiconductor and self-assembled-monolayer interfaces. *Phys. Rev. B* **73**, 193310. (doi:10.1103/PhysRevB.73.193310)
35. Heimel G, Romaner L, Brédas J-L, Zojer E. 2006 Organic/metal interfaces in self-assembled monolayers of conjugated thiols: a first-principles benchmark study. *Surf. Sci.* **600**, 4548–4562. (doi:10.1016/j.susc.2006.07.023)
36. Azzam W, Fuxen C, Birkner A, Rong H-T, Buck M, Wöll C. 2003 Coexistence of different structural phases in thioaromatic monolayers on Au(111). *Langmuir* **19**, 4958–4968. (doi:10.1021/la020868y)
37. Kresse G, Furthmüller J. 1996 Efficient iterative schemes for ab initio total-energy calculations using a plane-wave basis set. *Phys. Rev. B* **54**, 11 169–11 186. (doi:10.1103/PhysRevB.54.11169)
38. Kresse G, Joubert D. 1999 From ultrasoft pseudopotentials to the projector augmented-wave method. *Phys. Rev. B* **59**, 1758–1775. (doi:10.1103/PhysRevB.59.1758)
39. Bilić A, Reimers JR, Hush NS. 2002 Adsorption of pyridine on the gold(111) surface: implications for 'alligator clips' for molecular wires. *J. Phys. Chem. B* **106**, 6740–6747. (doi:10.1021/jp020590i)
40. Hou S, Ning J, Shen Z, Zhao X, Xue Z. 2006 Influences of the molecule-electrode interface structure on the conducting characteristics of the gold-4,4 bipyridine-gold molecular junction. *Chem. Phys.* **327**, 1–9. (doi:10.1016/j.chemphys.2006.02.013)
41. Heimel G, Romaner L, Brédas J-L, Zojer E. 2006 Interface energetics and level alignment at covalent metal-molecule junctions: π-conjugated thiols on gold. *Phys. Rev. Lett.* **96**, 196806. (doi:10.1103/PhysRevLett.96.196806)
42. Tonigold K, Groß A. 2010 Adsorption of small aromatic molecules on the (111) surfaces of noble metals: a density functional theory study with semiempirical corrections for dispersion effects. *J. Chem. Phys.* **132**, 224701. (doi:10.1063/1.3439691)
43. Tkatchenko A, Scheffler M. 2009 Accurate molecular van der Waals interactions from ground-state electron density and free-atom reference data. *Phys. Rev. Lett.* **102**, 073005. (doi:10.1103/PhysRevLett.102.073005)
44. Ruiz VG, Liu W, Zojer E, Scheffler M, Tkatchenko A. 2012 Density-functional theory with screened van der Waals interactions for the modeling of hybrid inorganic-organic systems. *Phys. Rev. Lett.* **108**, 146103. (doi:10.1103/PhysRevLett.108.146103)
45. Mishchenko A, Zotti LA, Vonlanthen D, Bürkle M, Pauly F, Cuevas JC, Mayor M, Wandlowski T. 2011 Single-molecule junctions based on nitrile-terminated biphenyls: a promising new anchoring group. *J. Am. Chem. Soc.* **133**, 184–187. (doi:10.1021/ja107340t)

46. Tkatchenko A, Romaner L, Hofmann OT, Zojer E, Ambrosch-Draxl C, Scheffler M. 2010 Van der Waals interactions between organic adsorbates and at organic/inorganic interfaces. *MRS Bull.* **35**, 435–442. (doi:10.1557/mrs2010.581)
47. Kang JF, Liao S, Jordan R, Ulman A. 1998 Mixed self-assembled monolayers of rigid biphenyl thiols: impact of solvent and dipole moment. *J. Am. Chem. Soc.* **120**, 9662–9667. (doi:10.1021/ja9811871)
48. Kümmel S, Kronik L. 2008 Orbital-dependent density functionals: theory and applications. *Rev. Mod. Phys.* **80**, 1. (doi:10.1103/RevModPhys.80.3)
49. Li Y, Lu D, Galli G. 2009 Calculation of quasi-particle energies of aromatic self-assembled monolayers on Au(111). *J. Chem. Theory Comput.* **5**, 881–886. (doi:10.1021/ct800465f)